# Simulation and theory of self-assembly and network formation in reversibly cross-linked equilibrium polymers

James T. Kindt[a)]
*Department of Chemistry and Cherry L. Emerson Center for Scientific Computation, Emory University, Atlanta, Georgia 30322*

(Received 7 June 2005; accepted 5 August 2005; published online 7 October 2005)

A simulation model of hard spheres capable of reversible assembly into chains, which then may reversibly cross-link into networks, has been studied through grand canonical Monte Carlo simulation. Effects of varying intra- and interchain bond strengths, chain flexibilities, and restrictions on cross-linking angle were investigated. Observations including chain-length distributions and phase separation could be captured in most cases using a simple model theory. The coupling of chain growth to cross-linking was shown to be highly sensitive to the treatment of cross-linking by chain ends. In some systems, ladderlike domains of several cross-links joining two chains were common, resulting from cooperativity in the cross-linking. Extended to account for this phenomenon, the model theory predicts that such cooperativity will suppress phase separation in weakly polymerizing chains and at high cross-link concentration. In the present model, cross-linking stabilizes the isotropic phase with respect to the nematic phase, causing a shift in the isotropic-nematic transition to higher monomer concentration than in simple equilibrium polymers. © *2005 American Institute of Physics*. [DOI: 10.1063/1.2046629]

## I. INTRODUCTION

Living cells maintain and adapt their internal structure through the reversible assembly of globular proteins into fibers and the cross-linking of fibers through the action of a range of specific agents.[1] Both the mechanical properties of these networks[2] and the thermodynamics of the aggregation process by which they are formed[3,4] have been topics of recent interest. Network formation by cytoskeletal components is an example of a reversible (or "physical") gelation transition, which has been widely studied in the context of synthetic polymers.[5,6] In contrast with most synthetic polymers, the length and stiffness of cytoskeletal fibers lead to long-ranged orientational correlations and tend to promote the formation of ordered phases.[3,4,7] A further contrast with physical gelation of typical synthetic polymers is that in "living networks" formed by cytoskeletal components, polymer lengths are not fixed but are subject to growth and dissociation concurrent with the reversible cross-linking; in this respect they show some similarity with networks formed from self-assembled micelles,[8] microemulsions,[9] block copolymers,[10] and dipolar chains.[11] In our previous simulation work,[12] we have treated equilibrium polymers that can form threefold ($T$ or $Y$-type) junctions. Zilman and Safran[13] have contrasted the phase behavior of such systems with those that exhibit reversible cross-linking (with fourfold $X$ junctions) and have described conditions favoring the association of stiff chains into bundles of aligned chains rather than networks.[7]

The present study addresses the coupling between chain length and cross-linking and the first-order gelation transition in equilibrium polymers with cross-links through Monte Carlo simulations of a simple model system in which the strength and angle specificity of both the chaining interactions and the cross-links can be easily varied. An analytical free-energy expression that is successful in accounting for simulation results is used to predict the phase-separation boundaries over a wide range of systems. Modifications to the analytical model are used to demonstrate the sensitivity to details of cross-link placement of the qualitative nature of the coupling between chain length and cross-linking. Under certain circumstances in which the cross-linking geometry promotes zipperlike structures, with multiple adjacent links between a given pair of chains, the phase separation shows reentrant behavior as the cross-linking strength (or activity of cross-linkers) is increased. While cross-linking interactions that restrict the angle between cross-linked chains are seen to promote long-ranged orientational order, when angle specificity is not included in the present model, cross-linking has the effect of stabilizing the isotropic phase under conditions where nematic ordering is observed in its absence.

## II. SIMULATION METHODS

### A. Coarse-grained simulation model

The simulation model is an extension of the sticky hard-sphere model used in a previous study on equilibrium polymerization.[14] Monomers are hard spheres of diameter $\sigma$, that reversibly form chains of neighboring monomers with neighbor bond distances constrained to equal $\sigma$ and bond angles restricted to the range $[\theta_{\min}, \pi]$. The persistence length of the chain is related to $\theta_{\min}$ as $l_p = 0.5(1+\cos\theta_{\min})$ at high $l_p$ (i.e., $\cos\theta_{\min}$ approaching $-1$). An association constant $K_{\mathrm{ch}}$ for the formation of a chain link in an ideal reference system is set as a parameter, in place of defining a bond

[a)]Electronic mail: jkindt@emory.edu

 

energy. In the present study, cross-links may be formed between any two monomers $i$ and $j$, as long as neither is a chain end or free monomer or is adjacent to another cross-linked monomer. (The restriction of cross-linking to chain interior monomers is intended to reflect cross-linking as a specific interaction, which would presumably be sensitive to conformational changes of the protein monomer during polymerization. The spacing restriction was imposed primarily for convenience in implementation, but is not unrealistic given the possibility of steric or electrostatic repulsions between cross-links.) Each monomer may form only one cross-link at a time. Upon cross-linking, the two monomers are constrained to a distance of one monomer diameter, i.e., $|\mathbf{r}_i-\mathbf{r}_j|=1$. The cross-linking angle $\theta_X$, defined as the angle between vectors $(\mathbf{r}_{i+1}-\mathbf{r}_{i-1})$ and $(\mathbf{r}_{j+1}-\mathbf{r}_{j-1})$, is restricted to a range $[\theta_{X.\min}, \theta_{X.\max}]$. Like the chaining potential, the cross-linking potential is effectively a square-well potential with infinitesimal thickness $\Delta$ and potential depth $\varepsilon_X$; an association factor $F_X=\Delta\exp(\beta\varepsilon_X)$ serves to control the strength of the cross-linking attractions.

### B. Monte Carlo algorithms

Biased grand canonical Monte Carlo (MC) simulations were used to sample this model potential. Three types of moves are employed: chain addition and removal/resizing using the polydisperse insertion, removal, and resizing (PDIRR) method,[14] and crankshaft moves. The strategy for forming and breaking cross-link bonds is similar to that used in Ref. 12: when an added or displaced monomer overlaps another monomer, an attempt is made to shift the monomer to a position satisfying the cross-link constraints with that target monomer.

The PDIRR algorithm comprises two types of move: aggregate insertion and aggregate removal/resizing. A general derivation of the method[15] and details of its application to the simple equilibrium polymer system[14] have been presented previously. Briefly, the chain insertion move consists of an initial monomer insertion followed by the directed, sequential addition of monomers to form a chain. The chain is allowed to grow until it reaches a limit to its growth, e.g., overlaps with a particle that is ineligible for cross-linking. At this point, an acceptance probability for the insertion of each intermediate in the chain growth is calculated and applied. The removal/resizing move involves calculation of weighting factors for intermediates in the stepwise disassembly of the aggregate as well as its further growth; based on the weighting factors for all of these structures, a decision is made either to remove the aggregate or to add or remove an arbitrary number of monomers.

During chain growth, addition of monomers to the chain end proceeds until an overlap with an existing monomer is found. In that case, an attempt is made to cross-link to the existing monomer. First, because multiple overlaps are possible, all $N_{\text{overlap}}$ potential target monomers must be determined, and one chosen at random to be the target. Cross-linking fails and the chain growth is stopped if the target is a free monomer, is a chain end, or is adjacent to an existing cross-link. The new position of the particle to be added must be at unit distance to both the target and the growing chain end; this restriction defines a circle of radius $(1-|\mathbf{u}|^2)^{1/2}$, where $2\mathbf{u}$ is the vector between the previous chain end and the target. The bond angle restrictions on the growing chain further restrict the locus of possible positions $\mathbf{r}_{i+1}$ for the added particle to the arc delimited by the intersection of this circle with a cone coaxial to $\mathbf{v}=(\mathbf{r}_i-\mathbf{r}_{i-1})\cos\theta_{\min}$, such that $(\mathbf{r}_{i+1}-\mathbf{r}_i)\cdot(\mathbf{r}_i-\mathbf{r}_{i-1})>\cos\theta_{\min}$. Defining $\mathbf{v}=(\mathbf{r}_i-\mathbf{r}_{i-1})\cos\theta_{\min}$, we find a vector perpendicular to $\mathbf{u}$;

$$\vec{q}\equiv\frac{\vec{\nu}\cdot\vec{\nu}-\vec{u}\cdot\vec{\nu}}{\vec{\nu}\cdot\vec{\nu}-[(\vec{u}\cdot\vec{\nu})^2/\vec{u}\cdot\vec{u}]}\left(\vec{\nu}-\frac{\vec{u}\cdot\vec{\nu}}{\vec{u}\cdot\vec{u}}\vec{u}\right). \tag{1}$$

The angle subtended by the arc is given by $2\alpha_{\text{lim}}$, where

$$\alpha_{\text{lim}}\equiv\arctan\sqrt{\frac{1-\vec{u}\cdot\vec{u}-\vec{q}\cdot\vec{q}}{\vec{q}\cdot\vec{q}}}. \tag{2}$$

A position satisfying distance and bond angle constraints is defined by the angle $\alpha$, chosen with uniform probability from the range $[-\alpha_{\text{lim}},\alpha_{\text{lim}}]$:

$$\vec{r}_{i+1}=\vec{r}_i+\vec{u}+\sqrt{1-\vec{u}\cdot\vec{u}}\left[\cos\alpha\frac{\vec{q}}{|\vec{q}|}+\sin\alpha\frac{\vec{u}\times\vec{\nu}}{|\vec{u}\times\vec{\nu}|}\right]. \tag{3}$$

If $\alpha_{\text{lim}}$ is not defined, then the angle range is either zero (usually) or $2\pi$. One way to check is to calculate $(\vec{u}+\sqrt{1-\vec{u}\cdot\vec{u}}|\vec{q}|^{-1}\vec{q})\cdot(\vec{r}_i-\vec{r}_{i-1})$; if the result is greater than $\cos\theta_{\min}$, then any point on the circle is acceptable, and $\alpha_{\text{lim}}$ should be set to $\pi$.

The volume of the target region is

$$\begin{aligned}V_{\text{site}}&=\Delta^2\left(2|\vec{u}|\sqrt{1-|\vec{u}|^2}\right)^{-1}\times\sqrt{1-|\vec{u}|^2}\times 2\alpha_{\text{lim}}\\&=|\vec{u}|^{-1}\alpha_{\text{lim}}\Delta^2.\end{aligned} \tag{4}$$

Since the model allows cross-links only between chain interior monomers, cross-link formation must fail if particle $i+2$ cannot also be added. That addition is made according to a normal biased addition scheme; if an overlap occurs, the addition of both $i+1$ and $i+2$ fails. After $i+2$ is added, any angle restrictions on the cross-link are tested. The absolute value of the cosine of the angle between the tangents to the two chains at the cross-linking points, i.e.,

$$\cos\theta_X=\frac{(\vec{r}_{i+2}-\vec{r}_i)\cdot(\vec{r}_{\text{target}+1}-\vec{r}_{\text{target}-1})}{|\vec{r}_{i+2}-\vec{r}_i||\vec{r}_{\text{target}+1}-\vec{r}_{\text{target}-1}|}, \tag{5}$$

must be within some predefined range. The PDIRR weight factor for the coupled steps of adding a cross-linked monomer and extending the chain one further is

$$\begin{aligned}W_{i+1,i+2}&=N_X\exp(2\beta\mu)K_{\text{chain}}^2\frac{V_{\text{site}}}{2\pi(1-\cos\theta_{\min})\Delta}\exp(\beta\varepsilon_X)\\&=N_X\exp(2\beta\mu)K_{\text{chain}}^2\frac{F_X\alpha_{\text{lim}}|\vec{u}|^{-1}}{2\pi(1-\cos\theta_{\min})},\end{aligned} \tag{6}$$

where we define $F_X=\Delta\exp(\beta\varepsilon_X)$. The ratio $V_{\text{site}}/[2\pi(1-\cos\theta_{\min})\Delta]$ accounts for entropy cost of restricting the range of positions from the target of a biased chain addition move without cross-linking (a truncated spherical shell) to the arc discussed above that additionally satisfies cross-linking. For addition to a free monomer, where no angle

TABLE I. Summary of Monte Carlo simulations. Simulation series performed, giving chain association constants, cross-linking factor, cross-link angle range, and box dimension. In most cases, multiple subseries were run at different persistence lengths, shown in column 6. The final column gives the chain association constant used in comparisons of simulation results with statistical theory.

| Series | $K_{ch}(\sigma^3)$ | $F_X(\sigma)$ | $[\theta_{X,min}, \theta_{X,max}]$ | $L_{box}(\sigma)$ | $l_p(\sigma)$ | $K_X(\sigma^3)$ |
|---|---|---|---|---|---|---|
| 1 | 320 | 50.26 | [25.84, 90] | 40 | 10 | 40 |
| 2 | 800 | 10.05 | [25.84, 90] | 40 | 4, 10, 1000 | 8 |
| 2b | 800 | 72.88 | [84.26, 90] | 40 | 10, 1000 | 8 |
| 2c | 800 | 145.77 | [25.84,36.87] | 40 | 10, 1000 | 8 |
| 3 | 5000 | 4.02 | [25.84, 90] | 40 | 10, 1000 | 3.2 |
| 3c | 5000 | 58.31 | [25.84,36.87] | 40 | 10 | 3.2 |
| 4 | 12,500 | 2.54 | [25.84, 90] | 50 | 10, 1000 | 2.02 |

restrictions are present, $2\pi(1-\cos\theta_{min})\Delta$ is replaced by $4\pi\Delta$.

The same weights must be calculated using Eq. (6) during the removal of a chain containing cross-linked monomers. If monomer $i+1$ is cross-linked, a dummy addition is made to particle $i$ to determine $N_X$; if $N_X=0$ then the removal move fails (but resizing may be attempted). Similarly, $\alpha_{lim}$ must be calculated to determine $V_{site}$.

Chain addition and removal/resizing moves are sufficient in principle to sample the system ergodically; however, for more efficient sampling of the interiors of chains, other moves are useful. We have used crankshaft moves in previous work on equilibrium polymers;[14] when no cross-links are involved, all crankshaft moves that produce configurations satisfying hard-sphere overlap and bond angle restriction are accepted. Here we derive acceptance probabilities for pivot moves that form and break cross-link bonds, consistent with our model. For simplicity, we allow only pivots of one monomer around the axis of its two neighbors on the same chain. Defining the distance between the two neighbors as $2d$, the range of motion describes a circle of radius $h=(1-d^2)^{1/2}$. A new position anywhere on this circle is first generated. If the position violates excluded-volume restrictions with one or more ($=N_{overlap}$) particles, then one of those particles is selected at random as the target for cross-linking, and one of the two intercepts of the circle with the sphere of unit radius centered on that particle is chosen for the trial position to accompany the creation of a cross-linking bond. Assuming a spherical shell of permitted positions with thickness $\Delta$, the arc falling within each point of interception is given by $\Delta/(h\cos\gamma)$, with $\gamma$ the angle between the normal to the shell and the tangent to the circle at the point of interception. The Boltzmann-weighted volume associated with the pair of binding positions is therefore $\omega_X=2A\exp(\beta\varepsilon_X)\Delta\sec\gamma=2A\sec\gamma F_X$, (with $A$ the cross-sectional area of the ring) and with the remaining position is $\omega_o=2\pi Ah$. If all other constraints—bond angle, cross-link angle, and excluded volume—are satisfied, then the acceptance probability for forming a cross-link during a pivot is

$$\mathrm{acc}=\min[1,N_{overlap}\omega_X/\omega_o]. \tag{7}$$

To satisfy detailed balance between cross-link forming and breaking moves, we must consider the probability of proposing the formation of a cross-link to a given target, which we call $\alpha_x$. To do so, when a pivot move is attempted on a cross-linked monomer and $N_{overlap}=0$ for the trial position, an independent "dummy" trial position is generated and the number of overlaps is counted. If one of the overlapping monomers is not the target, the move is rejected. Otherwise, the value of $N_{overlap}$ for the dummy position is used in the acceptance probability:

$$\mathrm{acc}=\min[1,N^{-1}_{overlap,dummy}\omega_o/\omega_x]. \tag{8}$$

The probability of proposing a cross-link formation move is therefore balanced with the probability of the removal move being allowed to proceed. Pivot moves of an already-cross-linked monomer for which $N_{overlap}>0$ can potentially lead to transfer of the cross-link from one target to another; these are subject to the same dummy trial position test and an acceptance probability,

$$\mathrm{acc}=\min[1,N_{overlap}\omega_{X,new}/(N_{overlap,dummy}\omega_{X,old})]. \tag{9}$$

Pivots between the two possible cross-linking positions on the same target monomer can be made with unit acceptance probability (subject to angle and excluded-volume constraints).

### C. Simulation details

Preliminary simulation results for stiff ($l_p=1000\sigma$) chains with unrestricted cross-linking angle showed a very strong tendency for pairs of chains to grow into long "railroad" structures with multiple consecutive cross-links. To prevent such structures, the minimum cross-link angle was set to 25.8 (i.e., $\cos\theta_x<0.9$). Four combinations of $K_{ch}$ and $F_x$ were initially investigated as listed in Table I as series 1–4. For each series, simulations of systems with $l_p=10\sigma$ ($\cos\theta_{ch}<-0.8$) and $l_p=1000\sigma$ ($\cos\theta_{ch}<-0.998$) were performed over a range of chemical potentials. Each simulation was performed for at least $2\times10^7$ PDIRR move attempts; convergence was evaluated by stabilization of the monomer and cross-linker concentrations and the chain-length distribution. All simulations were performed using a cubic simulation cell with periodic boundary conditions and constant box edge length $L_{box}$. The mean total monomer concentration $\rho\equiv N/V$, with $N$ the total number of monomers, along with mean concentrations of cross-links and chain-length distributions were monitored during the simulation runs, along with bond orientational distributions and chain angle distributions. In simulation production runs, PDIRR

and pivot moves were attempted with equal probabilities. Comparing results of trial simulations on small, rapidly equilibrated systems with and without pivot moves proved a sensitive test for bugs and inconsistencies in both algorithms. The final version of the code passed all such tests, giving superimposable histograms for the distributions of the number of particles, number of cross-links, number of chains, and cross-link angle distributions with or without the pivot moves. As both the derivations and implementations of the PDIRR and pivot move algorithms were entirely independent, the demonstration of consistency between the two is evidence for the soundness of both.

## III. THEORY

### A. Ideal statistics

If a monomer's cross-linking capability does not depend on whether it is part of a chain or on its position in that chain, then the polymerization equilibrium may be treated independently of the cross-linking equilibrium, and the association statistics and phase behavior are predicted[13] to follow the well-studied behavior of equilibrium polymers with isotropic attractions.[16]

The present simulation model's placement restrictions on cross-linked monomers, which prevent cross-linking by chain ends and neighbors of existing cross-links, require a self-consistent treatment of polymerization and cross-linking. We will proceed by formally treating the chain assembly and cross-linking as separate stages. It is convenient to define the first stage as the formation of chains by all monomers *not* involved in cross-links, forming a solution of free chains. As in previous approaches to equilibrium polymerization,[16] the free energy of each chain is given by a translational entropy term, related to the concentration $\rho_{S1,i}$ of chains of that length, and an internal bond free-energy term proportional to the number $i-1$ of bonds in the chain and the bond free energy $k_BT \ln K_{ch}$. The system's free energy associated with assembly into an ideal equilibrium polymer solution in this first stage is the sum over chain lengths $i$:

$$\beta f_{S1} = \sum_{i=1}^{\infty} \rho_{i,S1}(\ln \rho_{i,S1} - 1 - (i-1)\ln K_{ch}). \tag{10}$$

The second stage then consists of the insertion of the remaining monomers into those chains and their cross-linking. The position restrictions are then met if no more than one cross-linking monomer is inserted into each original bond of the chains formed in the first stage, of which there are $i-1$ for each chain of length $i$, for a total concentration of interior sites $\rho_{in}=\rho_{tot}-\rho_{ch}$. The formation of each cross-link involves the addition of two new particles, one on each linked chain to be linked, and the removal of two sites from availability. The equilibrium between open sites and cross-linked sites gives

$$K_X^* = \frac{\rho_X}{(\rho_{in}-2\rho_X)^2}, \tag{11}$$

which can be solved for the concentration of cross-links:

$$\rho_X = \frac{4\rho_{in}K_X^* + 1 - \sqrt{8\rho_{in}K_X^* + 1}}{8K_X^*}. \tag{12}$$

The effective cross-linking constant $K_X^*=K_X(K_{ch}\rho_1)^2$ accounts for both the insertion of free monomers into the two sites joined by each cross-link (for a net increase of two intrachain bonds) and the formation of the cross-link itself.

The free energy associated with allowing cross-links is determined from the binding free energy and the entropy associated with the number of unique cross-linking combinations. Each cross-link formed lowers the system's free energy by $k_BT \ln K_X^*$ while reducing the translational entropy of one of the chains involved in the cross-link by $k_B \ln V$. The number of ways to choose $N_X$ ordered pairs out of $N_{in}$ sites is $(N_{in}!)[(N_{in}-2N_X)!(N_X!)]^{-1}$. The entropy of mixing term is obtained by taking the logarithm and multiplying by $k_B$. Combining these terms, applying Stirling's approximation, and dividing through by volume yields the free-energy change per unit volume from cross-linking:

$$\beta f_X = -\rho_X \ln K_X^* - \rho_{in} \ln \rho_{in} + (\rho_{in}-2\rho_X)\ln(\rho_{in}-2\rho_X) + \rho_X(\ln \rho_X + 1). \tag{13}$$

Substitution of $\rho_X$ from Eq. (12) minimizes $f_X$ at constant $\rho_{in}$, as expected. The distribution of chain lengths in stage 1 is coupled to $f_X$ through $\rho_{in}$; to determine the optimum distribution of stage 1 chain lengths *before* the addition of cross-linked monomers requires finding $\rho_{S1,i}$ that satisfy

$$i\frac{\partial(f_{S1}+f_X)}{\partial\rho_{S1,1}} = \frac{\partial(f_{S1}+f_X)}{\partial\rho_{S1,i}}, \tag{14}$$

which gives

$$\rho_{S1,i} = \left[K_{ch}/(1-2\rho_X/\rho_{in})\right]^{i-1}\rho_1^i. \tag{15}$$

As each chain of length $i$ contributes $i-1$ sites towards $\rho_{in}$, $\rho_{in}$ can be obtained by substituting the $\rho_{S1,i}$ into a series expression:

$$\rho_{in} = \sum_{i=1}^{\infty}(i-1)\rho_{S1,i} = \frac{K_{ch}(1-2\rho_X/\rho_{in})^{-1}\rho_1^2}{\left[1-K_{ch}(1-2\rho_X/\rho_{in})^{-1}\rho_1\right]^2}, \tag{16}$$

which can then be solved for $\rho_1$ as

$$\rho_1 = \frac{\rho_{in}^{1/2}K_{ch}^{-1/2}\left[1-2\rho_X/\rho_{in}\right]^{1/2} - \rho_{in}}{1-K_{ch}\rho_{in}\left[1-2\rho_X/\rho_{in}\right]^{-1}}. \tag{17}$$

(Note that the concentration of free monomers is unaffected by the cross-linking stage, so $\rho_1=\rho_{S1,1}$.)

However, $\rho_X$ depends on $\rho_{in}$ and (through $K_X^*$) on $\rho_1$. A convenient numerical way to solve the combination of Eqs. (12) and (17) is to fix $\rho_{in}$ and solve iteratively and self-consistently for $\rho_1$ and $\rho_X$. Using the numerical results, we can find the concentration of chains:

$$\rho_{ch} = \sum_{i=1}^{\infty}\rho_{S1,i} = \frac{\rho_1}{1-K_{ch}\rho_1(1-2\rho_X/\rho_{in})^{-1}}. \tag{18}$$

The total monomer concentration before cross-linkers are added can be found by adding $\rho_{ch}$ to the concentration of original sites ($i-1$ per original chain) $\rho_{in}$. The total including cross-linking monomers is then

$$\rho_{\mathrm{tot}} = \rho_{\mathrm{in}} + \rho_{\mathrm{ch}} + 2\rho_X. \tag{19}$$

The mean chain length $M$ is defined as the ratio of $\rho_{\mathrm{tot}}$ to $\rho_{\mathrm{ch}}$. As monomers in all chains are at equilibrium, the monomer chemical potential for the ideal system is equal to the chemical potential of the free monomer, obtained by differentiation of Eq. (10) with respect to $\rho_{S1}$ (which equals $\rho_1$) to give $\mu_{\mathrm{ideal}} = k_B T \ln(\rho_1)$.[17]

### B. Cooperative cross-linking

Cooperativity is determined by the effective local concentration $J$ of next-nearest neighbors of an existing cross-linked pair for each other, enhanced by their proximity to the bond. The probability that a bond will form between the neighbors is then proportional to $K_X J$. We can treat cases of cooperative cross-linking, in which the presence of a cross-link between monomers on two chains increases the likelihood that the monomers' next-nearest neighbors will also be cross-linked, by treating it as a third stage in self-assembly. In this third stage, cross-links formed in the second stage, each of which is an independent junction between a different pair of chains, are converted into domains of multiple cross-links reinforcing the original junctions. In other words, the cross-link pairs themselves undergo a second equilibrium polymerization to form ladders. Each cross-link added to an existing domain requires four monomers (a spacers and a cross-linker on each chain) and yields four intrachain bonds and one interchain bond; the effective equilibrium constant for the extension of the domain is therefore $K_X J(K_{\mathrm{ch}}\rho_1)^4$ or $K_X^* J(K_{\mathrm{ch}}\rho_1)^2$. The average number of cross-link pairs in each sequence is then given by

$$\begin{aligned} L &= \left( \frac{1 + 2K_X^* J(K_{\mathrm{ch}}\rho_1)^2 + 3[K_X^* J(K_{\mathrm{ch}}\rho_1)^2]^2 \cdots}{1 + K_X^* J(K_{\mathrm{ch}}\rho_1)^2 + [K_X^* J(K_{\mathrm{ch}}\rho_1)^2]^2 \cdots} \right) \\ &= \left[1 - K_X^* J(K_{\mathrm{ch}}\rho_1)^2\right]^{-1}. \end{aligned} \tag{20}$$

To incorporate cooperativity into the original model, a renormalized equilibrium constant $LK_X^*$ is substituted for $K_X^*$ in Eqs. (12) and (13), the density of cross-links in the system is $L$ times the density $\rho_{S2,X}$ obtained in stage 2, and the total number of particles is similarly adjusted to include the extra cross-linkers and spacer monomers:

$$\rho_{\mathrm{tot}} = \rho_{\mathrm{in}} + \rho_{\mathrm{ch}} + 2\rho_{S2,X}(2L - 1). \tag{21}$$

### C. Excluded-volume effects

For an approximate treatment of excluded-volume interactions in the system, we add several terms to the free-energy density of the system:

$$\beta f_{\mathrm{xv}} = \tfrac{1}{2} B \rho_{\mathrm{tot}}^2 + \tfrac{1}{3} C \rho_{\mathrm{tot}}^3 + \kappa_1 \rho_{\mathrm{ch}} \rho_{\mathrm{tot}} - \kappa_X \rho_X \rho_{\mathrm{tot}}. \tag{22}$$

The first two terms on the right-hand side are second and third virial contributions, which are independent of the cross-linking and assembly and only add to the chemical potential. The third term, included in previous treatments of equilibrium polymers without cross-links,[14,18] represents the excluded-volume penalty to break a chain bond; an effective depletion force favors bonding in a crowded system, which has a significant effect on the growth law above $\rho_{\mathrm{tot}} = 0.1$. The fourth term corresponds to the same effect on the cross-link bond; the sign is reversed because $\rho_X$ counts bonds formed while $\rho_{\mathrm{ch}}$ counts bonds broken. The correct effect on the chaining and cross-linking equilibrium can be achieved by substituting $K_{\mathrm{ch}}^* = K_{\mathrm{ch}} \exp(\kappa_1 \rho_{\mathrm{tot}})$ for the chain association constant and $K_X^{**} = K_X \exp(\kappa_X \rho_{\mathrm{tot}})(K_{\mathrm{ch}}^* \rho_1)$ for $K_X^*$ in Eqs. (11)–(20). The chemical potential, obtained by adding the derivative of Eq. (22) with respect to $\rho_{\mathrm{tot}}$ to $\mu_{\mathrm{ideal}}$ is then

$$\beta\mu = \ln(\rho_1) + B\rho_{\mathrm{tot}} + C\rho_{\mathrm{tot}}^2 + \kappa_1(\rho_{\mathrm{ch}} + \rho_{\mathrm{tot}}) - \kappa_X \rho_X, \tag{23}$$

where $\rho_1$ is obtained from Eq. (17). As $\mu$ can be obtained as a continuous implicit function of $\rho_{\mathrm{tot}}$, where a loop develops in $\mu(\rho_{\mathrm{tot}})$ the coexistence boundaries for phase separation can be obtained through the Gibbs construction [i.e., $\mu(\rho_A) = \mu(\rho_B), \int_{\rho_A}^{\rho_B} \mu(\rho) d\rho = 0$].

### D. Chain-length distributions

While the distribution of chain-length concentrations following the first stage of assembly is known to be exponential based on Eq. (15), the chain-length distribution including the insertion of cross-linkers is no longer so simple. It is convenient to approach this problem by considering the equilibria involved in the disassembly of a chain of length $i > 2$ from one end. When the end is not adjacent to a cross-linked monomer, which will be true for some fraction $g_i$ of chains, the process involves simply breaking one bond and removing a monomer. Therefore:

$$g_i \rho_i = K_{\mathrm{ch}} \rho_{i-1} \rho_1. \tag{24}$$

For the remaining chains, breaking the last bond would leave a cross-linked monomer at the end, which is forbidden. Instead, the cross-linked monomer can be removed, leaving two un-cross-linked monomers (and one free cross-linking site) at the end. Thus, the remaining chains of length $i$ are at equilibrium with the same subset of chains of length $i-1$, which are present in a concentration $g_{i-1}\rho_{i-1}$. Assuming a statistical distribution of filled and free cross-linking sites as defined in Sec. III A, the ratio is also known:

$$(1 - g_i)\rho_i = 2\rho_X(\rho_{\mathrm{in}} - 2\rho_X)^{-1}(g_{i-1}\rho_{i-1}). \tag{25}$$

Adding Eqs. (24) and (25) yields a formula to generate $\rho_i$ from $\rho_{i-1}$ and $\rho_{i-2}$:

$$\begin{aligned} \rho_i &= K_{\mathrm{ch}} \rho_{i-1} \rho_1 + 2\rho_X(\rho_{\mathrm{in}} - 2\rho_X)^{-1}(g_{i-1}\rho_{i-1}) \\ &= K_{\mathrm{ch}} \rho_1 [\rho_{i-1} + 2\rho_X(\rho_{\mathrm{in}} - 2\rho_X)^{-1}\rho_{i-2}]. \end{aligned} \tag{26}$$

For cooperative cross-linking, where the second equilibrium involves removing a series of cross-links of variable length, this becomes

$$\rho_i = K_{\mathrm{ch}} \rho_{i-1} \rho_1 + \rho_i = K_{\mathrm{ch}} \rho_1 \left[ \rho_{i-1} + \sum_{j=0}^{(i-3)/2} 2\rho_X(\rho_{\mathrm{in}} - 2\rho_X)^{-1} \rho_{i-2-2j} L^{-1}(1 - L^{-1})^j \right]. \tag{27}$$

### E. Parameter selection for comparison with simulations

The chain association constant $K_{ch}$ as defined in the simulation model can be used directly in the theory. Parameters for the first three terms in Eq. (22) were obtained from simulation data of the system without cross-links. (A new fit for $B$ and $C$ was performed using data from Ref. 14, yielding $B=1.3\sigma^3$ and $C=4.5\sigma^6$, while the value $\kappa_1=1.45\sigma^3$ was used unchanged.) In principle, the relationship between $F_X=\Delta\exp(\beta\varepsilon_X)$ and $K_X$ is found by multiplying $F_X$ by the surface area of a monomer, $4\pi\sigma^2$, times the average fraction of the surface area accessible for contact between two chain interior monomers. While this fraction can be estimated numerically for ideal cases, and is of order $10^{-1}$, instead we selected $K_X=8$ to give the best fit to a subset of the simulation data (series 2, $l_p=1000\sigma$, $\rho_x$ vs $\rho$ in the limit of low $\rho$), and scaled to $F_X$ for series 1, 3, and 4 as shown in Table I. Introduction of the final parameter, $\kappa_X=2.9\sigma^3$, was necessary to obtain good agreement with the same simulation data set at high $\rho$, and was kept fixed for all other data sets.

## IV. RESULTS AND DISCUSSION

### A. Degree of cross-linking

The rise in cross-link concentration $\rho_X$ with total monomer concentration $\rho$ from simulation (symbols) and theory (curves) is shown in Fig. 1(a). At low concentrations, $\rho_X$ increases as approximately the square of $\rho$, as expected for pairwise attractions. The restriction that each monomer may only form one cross-link and that neighboring monomers on a chain may not both be cross-linked defines a saturation limit of $\rho_X=\rho/4$, and $\rho_X$ increases more nearly linearly with $\rho$ once it reaches a significant fraction of this limit. With two adjustable parameters, $K_X$ and $\kappa_X$ optimized with data from series 2, the theory described in Sec. III A is quantitatively successful in describing three further sets of data (where $K_X$ is scaled linearly with the $F_X$) without further adjustment.

### B. Coupling between chain length and cross-linking

The agreement between simulation and theory extends to prediction of the mean chain length as well as the cross-link density, as shown in Fig. 1(b). In the simulation model, a free monomer or a monomer at a chain end cannot maintain a cross-link. This prohibition couples chain growth to cross-linking; a cross-linked chain is restricted in how it can disassemble without breaking the cross-link. In a hypothetical system where chain ends and free monomers can cross-link equally as well as chain interior particles, then this coupling is removed, and the chain-length distribution will be the same (within the mean-field approximation) in the presence and absence of cross-linkers.

More generally, the degree and sign of the coupling between chain growth and cross-linking depends on the details of how the number of cross-linking sites on a chain depends on the chain length. In the present simulation model, the number is $(i-1)/2$, rounded down for even $i$; breaking a bond removes, on average, $1/2$ of a cross-linking site. We

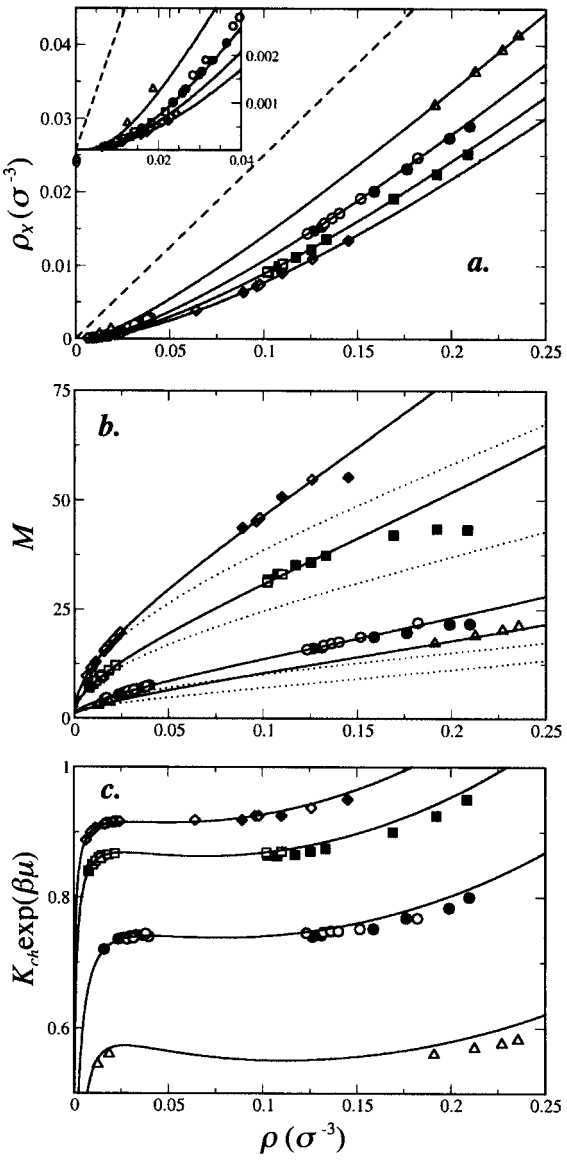


FIG. 1. Comparison of simulation (symbols) with theory (solid curves) for cross-link density $\rho_X$ (panel a), mean chain length $M$ (panel b), and scaled monomer activity $K_{ch}\exp(\beta\mu)$ (panel c). Persistence length of chains is indicated by open ($l_p=10\sigma$) or closed ($l_p=1000\sigma$) symbols. Data from systems with increasing $K_{ch}$ and decreasing $K_X$, defined as series 1, 2, 3, and 4 in Table I, are represented with triangles, circles, squares, and diamonds, respectively. The dashed line in panel a represents the saturation limit $\rho_X=\rho/4$ and the dotted curves in panel b represent the model prediction in the absence of cross-links.

consider two alternative models. In model I, the restriction on cross-linking to any neighbor of an already-cross-linked monomer is relaxed, but the prohibition on end monomers forming bonds is maintained, then the number becomes $i-2$; breaking a bond to form two new ends then removes two cross-linking sites. In model II, the spacing requirement is preserved but end monomers are permitted to cross-link; then $(i+1)/2$ (rounded down) cross-links may form per chain, and breaking a chain will in some cases add a new cross-linking site. While Monte Carlo results have only been obtained for the original case, analyses of the other models (detailed in the Appendix ) predict qualitatively different behavior in the other cases, as shown in Fig. 2. A much more

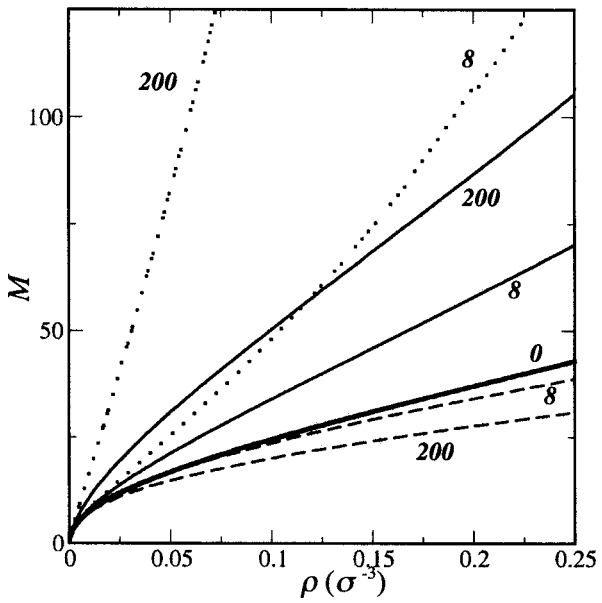


FIG. 2. Theoretical predictions of the influence of cross-linking constant $K_X$ on growth law (mean chain length $M$ vs total monomer concentration $\rho$). Three models are represented: simulation model (solid curves), alternative model I (dotted curves), and alternative model II (dashed curves). The heavy solid curve shows the growth law without cross-linking (same for all models) at $K_{ch}=5000\sigma^3$. The labels indicate the values of $K_X$ in $\sigma^3$.

dramatic positive coupling of chain length to cross-linking strength is seen in the second case, and a decrease in chain length with increasing $K_x$ is seen in the third case. A qualitative interpretation of this negative correlation is that repulsions among cross-linkers (e.g., polyvalent ions[19]) will tend to lower the effective chain association constant.

The distribution of chain lengths, like the mean chain length, is influenced by effects of cross-linking, particularly for short chains. In the present model, the spacing requirements of cross-links lead to an alternating distribution pattern, with chains of odd length more common than chains of even length. This pattern can be generated using Eq. (26) and the parameters fit to the mean-field theory, giving good agreement with simulation as shown in Fig. 3 for a typical case.

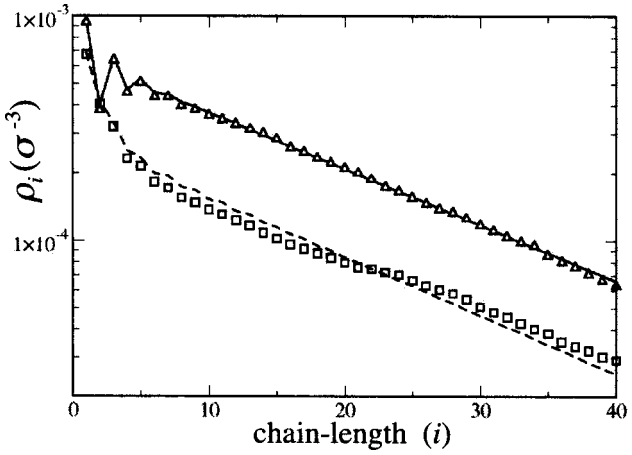


FIG. 3. Chain-length distributions from two simulations, with fits from Eqs. (26) and (27). Triangles: series 2, $l_p=10\sigma, \rho=0.191\sigma^{-3}$; Squares: series 2c, $l_p=10\sigma, \rho=0.079\sigma^{-3}$.

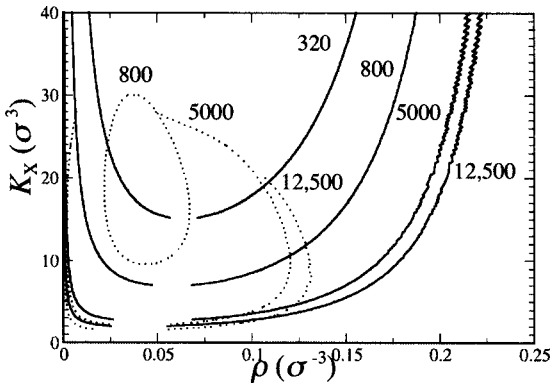


FIG. 4. Theoretically predicted coexistence boundaries for simulation model. Curves are labeled with $K_{ch}$ in $\sigma^3$. Solid curves: no cooperativity; dotted curve: $J=3.2\sigma^{-3}$.

### C. Phase separation

The systems selected for simulation each show a first-order gelation transition, as evident from the discontinuities in the isotherms of chemical potential versus density in Fig. 1(c). The concentrations of the two phases at coexistence are bounded, in each case, by the range of chemical potentials for which both dilute and gel phases are metastable. The coexistence points can be determined precisely by combining this data with pressure/density isotherms; however, determining pressures in this type of system is difficult.[14] Instead, relying on the successful fitting of the simulation data by the statistical thermodynamic model, we use the model to predict the boundaries of the region of phase separation as a function of $K_X$ at each value of $K_{ch}$, shown in Fig. 4. The trend that the critical point shifts to lower monomer concentration and lower $K_X$ as $K_{ch}$ increases is well known, and can be explained through modifications to the Flory-Huggins theory.[16]

In the present simulation model, $K_X$ is treated as an association constant proportional to the logarithm of the free energy of a cross-link bond, without explicitly defining a cross-linking agent as a distinct species. However, where cross-linking is a ternary interaction between involving two chain sites and a mobile cross-linker with association constant $K_{X,tern}$, the binary association constant $K_X$ may be substituted by $K_{X,tern}\rho_{free\text{-}Xlinker}$. The phase diagram represented in terms of $K_X$ thus may be applied as well to the phase behavior of a system with reversibly binding cross-linkers as the concentration (or more precisely the activity) of free cross-linkers is varied at constant cross-linking energy.

### D. Cross-link angle distribution

The distribution of cross-link angles $\theta_X$ is shown for typical simulations at two values of $\rho$ and $l_p=10\sigma$ and $l_p=1000\sigma$ in Fig. 5. (Note that the distribution falls to zero above $\cos\theta_X=0.9$, in accordance with the angle range restriction listed in Table I.) Random pairing between isotropically oriented chains would result in a uniform distribution of cross-links as a function of $\cos\theta_X$. In contrast, a significant drop in cross-linking probability is observed in the simulations at large $\cos\theta_X$ (i.e., more nearly parallel chains). To explain the observed angle distribution we consider the packing of tangent hard-sphere chains at contact. When a

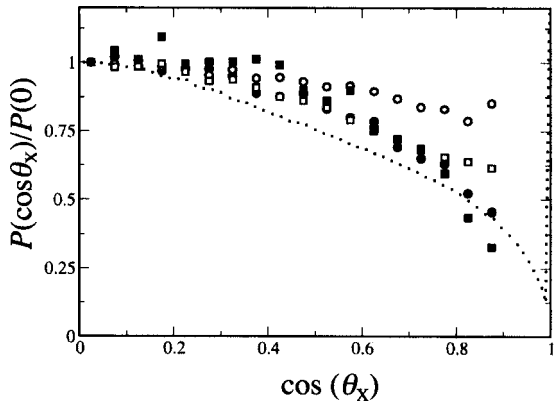


FIG. 5. Cross-link angle distribution, normalized to a probability of 90 deg. cross-links. Filled symbols: series 4, $l_p=1000\sigma$. Circles: $\rho=0.009\sigma^{-3}$; squares: $\rho=0.11\sigma^{-3}$. Open symbols: series 4, $l_p=10\sigma$. Circles: $\rho=0.018\sigma^{-3}$; squares: $\rho=0.126\sigma^{-3}$. Dotted line: distribution predicted for straight, rigid trimers.

cross-link forms, a monomer on one chain must be in contact with a monomer on another without their neighbors overlapping; qualitatively, neighbors are more distant and less likely to overlap at large cross-link angles. The fraction of the surface that satisfies this condition was computed numerically as a function of cross-link angle for the simple case of two perfectly straight trimeric chains, and drops off with increasing cos $\theta_X$ as shown by the dashed curve in Fig. 5.

The Monte Carlo data from full simulations show a similar but less dramatic drop in binding probability for angles near parallel orientations. Much of the difference may be attributed to flexibility effects; neighbors to cross-linked monomers have more freedom to avoid overlap in more flexible chains. At $l_p=10\sigma$, the fraction of near-parallel cross-links is significantly higher for low $\rho$ than for high $\rho$, an effect which is likely the result of cooperative cross-linking as described below. The angle dependence is apparently, therefore, specific to the present model and would be quite different if cross-linked chains were offset from each other by a distance comparable to the chain diameter by a linker molecule.

Further investigation of the effects of chain flexibility and cross-linking angle has been undertaken at chaining and cross-linking strengths corresponding to series 2. ($K_{\mathrm{ch}}=800\sigma^3$ and $K_X=8\sigma^3$). Lowering the persistence length to $l_p\approx 4\sigma, (\theta_{\min}=\pi/2)$ has little effect on chain-length distribution and cross-link concentration at a given $\rho$, but raises the overall chemical potential and suppresses the phase separation (Fig. 6 gray circles). Intrachain repulsion causes the increase in chemical potential, while competition from intrachain "looping" cross-links weakens the effective interchain attraction enough to suppress the first-order condensation transition under the current conditions. This effect of flexibility on gelation has been addressed in previous theoretical treatments of polymer gelation[5] and demonstrated in simulations of network formation with threefold junctions.[12]

A trivial effect of decreasing range of allowed cross-linking angles is to decrease the effective cross-linking constant. Increased cross-linking factors $F_X$ were chosen to compensate for this trivial effect, and highlight the effects of structural correlations arising from the cross-linking angle, in simulations in which $\theta_X$ was restricted to near 90 (series 2b) or near 30 (series 2c). The new values of $F_X$, shown in Table I, were selected to give agreement with series 2 in $\rho_X$ at low $\rho$. For stiff chains, phase separation is observed made in each case between a dilute isotropic phase and an orientationally ordered gel, having trigatic and tetratic symmetry, respectively.[3] The activity isotherms for both these transitions, shown in Fig. 6(c), show significantly wider coexistence regions than for isotropic phase separation. The investigation of these and other liquid crystalline phases that arise from restrictions in $\theta_X$ is in progress and will be presented fully in a later report.

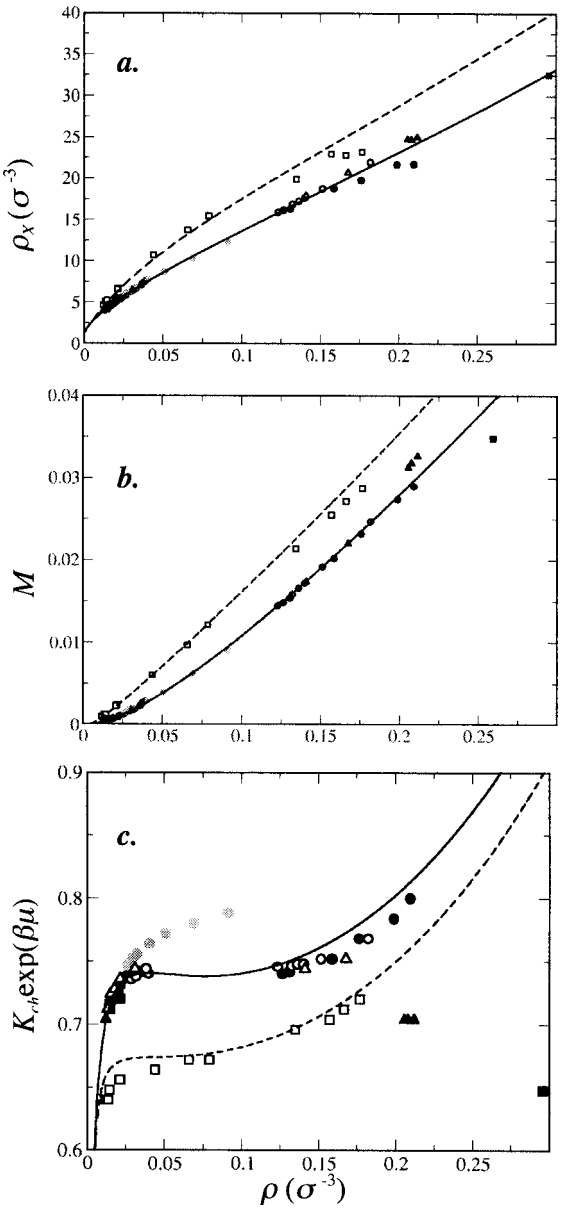


FIG. 6. Comparison of simulation (symbols) with theory (solid curves: same as Fig. 1; dashed curves: $J=3.2\sigma^{-3}$) for cross-link density $\rho_X$ (panel a), mean chain length $M$ (panel b), and scaled monomer activity $K_{\mathrm{ch}}\exp(\beta\mu)$ (panel c). Series 2: circles; series 2b (cross-link angles near 90): triangles; series 2c (cross-link angles near 30): squares. Filled symbols: $l_p=1000\sigma$; open symbols: $l_p=10\sigma$; gray symbols: $l_p=4\sigma$.

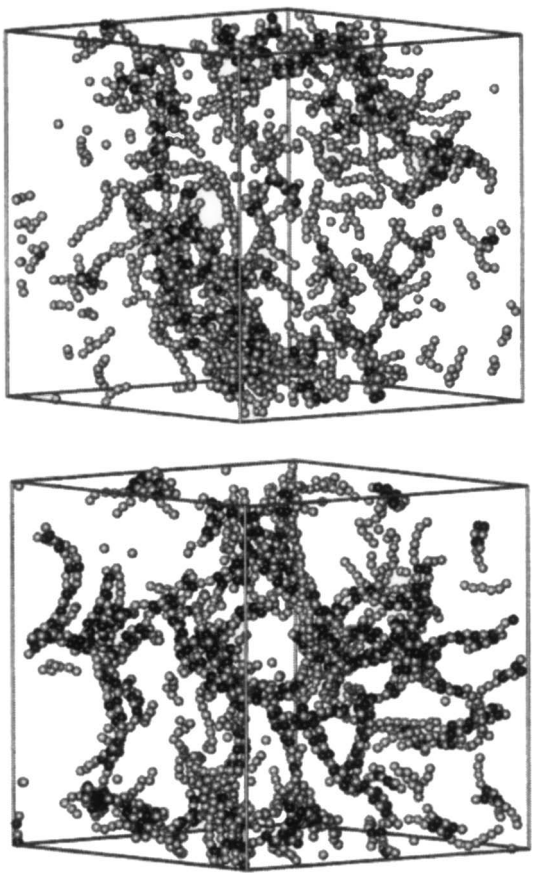

FIG. 7. Snapshots from simulations at $\rho=0.03\sigma^{-3}$. Upper: series 2, $l_p=10\sigma$. Lower: series 2c, $l_p=10\ \sigma$. Cross-linked pairs of monomers are highlighted in black.

### E. Cooperative cross-linking

More flexible chains ($l_p=10\sigma$) do not maintain orientational correlations between cross-links strongly enough to form ordered phases under the present conditions. Chain growth and network formation are not qualitatively affected by restriction of cross-link angles for cross-links near 90 (Fig. 6, open triangles). In contrast, when the restriction to angles near 30 is imposed (Fig. 6, open squares), strong deviations in all measures were seen: higher cross-link concentrations, greater mean chain lengths, lower chemical potentials, and no phase separation. Comparison of simulation snapshots in Fig. 7 from series 2 (upper image) and 2c (lower image) suggests that the ladderlike, or zipperlike domains in the latter as the apparent cause. For this combination of the bond and cross-link angle distribution, each cross-link bridging two chains preorganizes nearby sections of the chain into favorable positions for cross-linking, effectively nucleating a double-stranded cooperatively cross-linked domain. (Similar structures and behavior are obtained at $l_p=1000\sigma$ when the cross-linking between parallel chain is allowed.)

Cooperative cross-linking can be accounted for in the statistical thermodynamic theory with one adjustable parameter, $J$, corresponding to the effective local concentration of cross-linking sites on the same chains adjacent to an existing cross-linker. For fairly rigid chains restricted to high cross-linking angles, $J$ will be effectively zero. The chain-length distribution, cross-link density, and $\mu$ vs $\rho$ isotherm for series 2b can be fitted fairly well through the statistical thermodynamic theory [Figs. 6(a)–6(c), open squares/dashed curves] with $J=3.2\sigma^{-3}$. The origins of such a large effective concentration are worth noting. For monomers $i$ and $j$ cross-linked together with a typical $\theta_X$ of $\cos^{-1}(0.85)$, the probability of finding monomer $i+2$ at distance $\sigma\pm0.005$ from monomer $j+2$ is approximately 0.004, corresponding to a local concentration of $0.003\sigma^{-3}$ near contact. The reduction of steric and orientational restraints can each account for roughly an order of magnitude in increasing the effective concentration of $i+2$ for $j+2$, relative to a site on a randomly oriented third chain. We have seen already in Sec. III E that in cross-linking of randomly oriented chains, steric effects reduce the accessible surface area of cross-linking sites by a factor of 10. In the present case, with the chains crossed at a low angle and with the monomers lining up roughly in register, steric exclusion will be much less probable. Even when contact is possible, based on Fig. 5 we can estimate that the cross-linking angle restriction for series 2b (with $\cos\theta_X$ allowed only between 0.8 and 0.9) will exclude about 95% of potential cross-links formed between chains in isotropic solution. The proportion will be much lower for monomers $i+2$ and $j+2$ because of the constraints on the cross-link angle formed by $i$ and $j$. The real local concentration of $\sim0.03\sigma^{-3}$ therefore translates to a hundred-fold higher effective local concentration, relative to free sites on independent chains.

The mean zipper domain size $L$ depends on $J$, the total monomer concentration, and the chain association constant; it will typically increase at small $\rho$, as chains grow longer, and then decrease at larger $\rho$ as the cross-linking site concentration from other chains becomes more significant compared with $J$. The effect of cooperativity on chain length holds no matter whether chain end monomers may form cross-links. The chain-length distribution in a system exhibiting cooperative cross-linking, shown as squares in Fig. 3, still shows some enhancement at odd lengths but also exhibits two decay constants corresponding roughly to paired and unpaired chains.

Cooperativity promotes phase separation in some circumstances, by enhancing the effective strength of the cross-linking interaction, and suppresses it in others, by removing available sites for further branching. Figure 4 gives a comparison of the coexistence boundaries in the presence (dotted curves, $J=3.2\sigma^{-3}$) and absence (solid curves) of cooperative cross-linking. The formation of multiple bonds enhances the effective strength of the cross-linking interaction, but leaves "zipped" chain pairs with few sites available for cross-linking other chains and forming a network. When chains are long enough to accommodate multiple cooperatively cross-linked domains, as observed at high $K_{\mathrm{ch}}$ (12 500 and $5000\sigma^3$) and low $K_X$, phase separation is enhanced and the coexistence region is extended to lower $K_X$ than without cooperativity. As $K_X$ increases, so does the domain size $L$, so that each chain will interact with fewer other chains and the phase coexistence region narrows and ends at a second critical point. For the shorter chains formed in systems with lower $K_{\mathrm{ch}}$, the coexistence region of the phase diagram is

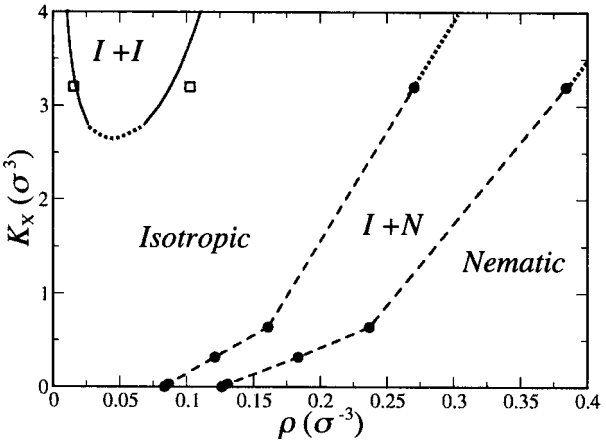


FIG. 8. Effect of cross-linking on nematic ordering transition, at $K_{ch}=5000\sigma^3$ and $l_p=1000\sigma$. The circles connected by dashed lines represent approximate coexistence boundaries (±5%) of isotropic and nematic phases from simulation. Coexistence boundaries for isotropic phase separation are shown as solid curves (from theory) and squares [estimated from $\mu$ vs $\rho$ simulation data for series 3 shown in Fig. 1(c)].

greatly reduced ($K_{ch}=800\sigma^3$) or suppressed altogether ($K_{ch}=320\sigma^3$). Phase separation was observed in series 3c (data not shown) in contrast to series 2c [see Fig. 6(c)], confirming the qualitative lesson from Fig. 4 that cooperativity suppresses phase separation in the low $K_X$ regime for low $K_{ch}$ but not for high $K_{ch}$. The prediction that cooperativity suppresses phase separation at high $K_X$ is quite reasonable, but was not amenable to testing by simulation due to slow equilibration of systems with long, strongly cross-linked double-stranded chain pairs.

An increase in the number of cross-linking sites upon alignment has been invoked by Zilman and Safran[7] to explain bundle formation in cross-linked actin. The cooperative formation of "zipper" domains discussed above can be considered a precursor to the formation of bundles of aligned chains. Further assembly into bundles is not advantageous in the simulation model, however, because pairing of chains allows occupation of all cross-linking sites; relaxing the restriction of one cross-link per monomer would seem to be a prerequisite for bundle formation under the present conditions.

### F. Nematic ordering

The present hard-sphere equilibrium polymer model has been shown previously to form a nematic phase in the absence of cross-linking.[14] In the present models (series 1–4), the tendency for stiff chains to align locally into bundles or globally into a nematic phase has been thwarted by the minimum cross-linking angle $\theta_X$ of 26. If this minimum is lowered to 11.5, stable nematic phases are observed, but with the minimum stable nematic phase concentration $\rho_N$ shifted upwards (to an extent that increases with $F_X$) from the value obtained in the absence of cross-linking, as shown in Fig. 8. The driving force for the $I-N$ transition in the absence of cross-links, within the framework of Onsager's theory,[20] is the reduction of excluded volume associated with the overlap of pairs of hard rods; each pair of rods gives a positive contribution to the second virial coefficient that scales as $L_iL_j\sigma|\sin\gamma_{ij}|$. However, each potential overlap is also an opportunity to form a cross-link, an effective attraction that provides a negative contribution to the second virial coefficient[13] with (in the present model) a similar angle-dependent scaling, shown in Fig. 5. The steric benefit to nematic ordering is therefore mitigated by the loss of opportunities for cross-linking. At high cross-link formation constant $K_X$, the transition is between two highly cross-linked phases and takes place at a significantly higher monomer concentration than the gelation transition. If the angle dependence of the cross-linking strength did not disfavor parallel chains, chain bundling or a combined gelation and ordering transition would be expected, similar to the behavior of series 2a and 2b.

The nematic order parameter $S$ of the nematic phase near coexistence shows little variation as $K_X$ increases, staying between 0.88 and 0.90 even as the total monomer density increases to nearly $0.4\sigma^{-3}$; in contrast, previous work has shown that increasing $\rho$ to just $0.17\sigma^{-3}$ (at the same $K_{ch}$ and $l_p$) in the absence of cross-linking brings $S$ up to 0.94.[14] The reduction of nematic order by cross-linking in the present model is consistent with the observation that cross-linking favors large angles.

## V. SUMMARY

Gelation through reversible cross-linking in a simple equilibrium polymer model has been investigated through Monte Carlo simulation. The behavior of the simulation model was well described using a system of equilibrium equations derived from an analytic free-energy expression. The most notable results were that the influence of cross-linking on mean chain length is sensitive to whether free monomers and chain ends can participate in cross-linking, and also to short-ranged repulsions between cross-links; if polymerization is a prerequisite for cross-linking, then the addition of cross-links will drive further polymerization, while repulsions between cross-linkers may moderate this effect. Cooperativity in cross-linking, observed under circumstances where the cross-linking of two monomers puts their neighbors in position to cross-link as well, is a strong promoter of chain growth. Because each monomer is only allowed to form one cross-link, cooperativity leads to ladder-like or zipperlike pairs of chains with few monomers available for further cross-linking, and tends to suppress the collective attractive driving force for phase separation. In the present model, the isotropic-nematic transition is shifted to higher monomer concentration as cross-linking strength increases, a result most likely arising from local packing effects specific to the hard-sphere model that disfavors cross-linking of nearly parallel chains.

## ACKNOWLEDGMENTS

This work was supported by National Science Foundation Grant No. CHE-0316076. Acknowledgment is made to the Cherry L. Emerson Center for Scientific Computation of Emory University for the use of its resources.

## APPENDIX: EQUILIBRIUM RELATIONS FOR ALTERNATIVE MODELS

Equations to solve for cross-link concentrations, mean chain lengths, and chemical potentials for variants of the simulation model used in generating Fig. 2 are included here. In alternative model I, all internal chain monomers are permitted to form cross-links. (This differs from the simulation model in the lack of restrictions on the spacing of cross-linked monomers.) The theory is simplified in that there is no need to couple cross-linking with inserting particles into the chain; Eq. (12) holds with $K_X^*=K_X$. The number of sites on a chain of length $i$ becomes $(i-2)$ rather than $(i-1)$. Equations (15) and (16) become

$$\rho_i = \rho_1^i K_{\mathrm{ch}}^{i-1}[1-2\rho_X/\rho_{\mathrm{in}}]^{-(i-2)} \tag{A1}$$

and

$$\rho_{\mathrm{in}} = \sum_{i=3}^{\infty}(i-2)\rho_i = \frac{K_{\mathrm{ch}}^3[1-2\rho_X/\rho_{\mathrm{in}}]^{-1}\rho_1^3}{\left(1-K_{\mathrm{ch}}[1-2\rho_X/\rho_{\mathrm{in}}]^{-1}\rho_1\right)^2}, \tag{A2}$$

from which $\rho_1$ may be obtained as a root of the cubic equation:

$$K_{\mathrm{ch}}^3(1-2\rho_X/\rho_{\mathrm{in}})^{-1}\rho_1^3 - K_{\mathrm{ch}}^2(1-2\rho_X/\rho_{\mathrm{in}})^{-2}\rho_{\mathrm{in}}\rho_1^2 + 2K_{\mathrm{ch}}(1-2\rho_X/\rho_{\mathrm{in}})^{-1}\rho_1 - \rho_{\mathrm{in}} = 0. \tag{A3}$$

Once $\rho_{\mathrm{in}}, \rho_X$, and $\rho_1$ have been determined self-consistently, the total monomer concentration and mean chain length are

$$\rho_{\mathrm{ch}} = \sum_{i=1}^{\infty}\rho_i = \rho_1 + \frac{K_{\mathrm{ch}}\rho_1^2}{1-K_{\mathrm{ch}}[1-2\rho_X/\rho_{\mathrm{in}}]^{-1}\rho_1},$$
$$\rho_{\mathrm{tot}}M = \rho_{\mathrm{in}} + 2\rho_{\mathrm{ch}} - \rho_1. \tag{A4}$$

The chemical potential of the ideal system remains $k_{\mathrm{B}}T\ln(\rho_1)$.

In alternative model II, monomers in all chains (but not free monomers) may form cross-links, but there must be at least one uncross-linked monomer between any two cross-linked monomers on the same chain. In this case, the effective number of bonding sites for chains of $i$ monomers assembled in the first stage is $i+1$, as a cross-linked particle can be added to each end. An important implication is that a distinction must be made between monomers that are free at the end of stage 1 and monomers that are free after the insertion of cross-linking monomers: $\rho_1=\rho_{\mathrm{S1},1}(1-2\rho_X/\rho_{\mathrm{in}})^2$. In calculating $K_X^*$ and $\mu, \rho_1$ must be used. Equivalents to Eqs. (15)–(19) are

$$\rho_{\mathrm{S1},i} = \rho_{\mathrm{S1},1}^i K_{\mathrm{ch}}^{i-1}(1-2\rho_X/\rho_{\mathrm{in}})^{i-1},$$

$$\rho_{\mathrm{in}} = \sum_{i=1}^{\infty}(i+1)\rho_{\mathrm{S1},i} = K_{\mathrm{ch}}^{-1}(1-2\rho_X/\rho_{\mathrm{in}})^{-1}\left[\left(1-K_{\mathrm{ch}}(1-2\rho_X/\rho_{\mathrm{in}})\rho_{\mathrm{S1},l}\right)^{-2} - 1\right],$$

$$\rho_{\mathrm{S1},1} = \frac{1-\left[1+K_{\mathrm{ch}}\rho_{\mathrm{in}}(1-2\rho_X/\rho_{\mathrm{in}})\right]^{-1/2}}{K_{\mathrm{ch}}(1-2\rho_X/\rho_{\mathrm{in}})}, \tag{A5}$$

$$\rho_{\mathrm{ch}} = \sum_{i=l}^{\infty}\rho_i = \frac{\rho_{\mathrm{S1},1}}{1-K_{\mathrm{ch}}[1-2\rho_X/\rho_{\mathrm{in}}]\rho_{\mathrm{S1},1}}$$

$$\rho_{\mathrm{tot}} = \rho_{\mathrm{in}} - \rho_{\mathrm{ch}} + 2\rho_X.$$

The systems of Eqs. (A1)–(A5) may be solved using the same approach and by introducing the same excluded-volume effects, as for the simulation model discussed in Sec. II.


[1] B. Alberts, A. Johnson, J. Lewis, M. Raff, K. Roberts, and P. Walter, *Molecular Biology of the Cell*, 4th ed. (Garland Science, New York, 2002).
[2] D. H. Boal, *Mechanics of the Cell* (Cambridge University Press, New York, 2002); D. A. Head, A. J. Levine, and F. C. MacKintosh, Phys. Rev. E **68**, 061907 (2003); M. L. Gardel, J. H. Shin, F. C. MacKintosh, L. Mahadevan, P. Matsudaira, and D. A. Weitz, Science **304**, 1301 (2004).
[3] R. F. Bruinsma, Phys. Rev. E **63**, 061705 (2001).
[4] I. Borukhov, R. F. Bruinsma, W. M. Gelbart, and A. J. Liu, Proc. Natl. Acad. Sci. U.S.A. **102**, 3673 (2005).
[5] A. N. Semenov and M. Rubinstein, Macromolecules **31**, 1373 (1998); A. V. Dobrynin, *ibid.* **37**, 3881 (2004).
[6] M. Rubinstein and A. V. Dobrynin, Curr. Opin. Colloid Interface Sci. **4**, 83 (1999); I. Erukhimovich and A. V. Ermoshkin, J. Chem. Phys. **116**, 368 (2002); S. K. Kumar and A. Z. Panagiotopoulos, Phys. Rev. Lett. **82**, 5060 (1999); S. K. Kumar and J. F. Douglas, *ibid.* **87**, 188301 (2001).
[7] A. G. Zilman and S. A. Safran, Europhys. Lett. **63**, 139 (2003).
[8] T. J. Drye and M. E. Cates, J. Chem. Phys. **96**, 1367 (1992).
[9] T. Tlusty, S. A. Safran, and R. Strey, Phys. Rev. Lett. **84**, 1244 (2000).
[10] S. Jain and F. S. Bates, Science **300**, 460 (2003).
[11] T. Tlusty and S. A. Safran, Science **290**, 1328 (2000).
[12] J. T. Kindt, J. Phys. Chem. B **106**, 8223 (2002).
[13] A. G. Zilman and S. A. Safran, Phys. Rev. E **66**, 051107 (2002).
[14] X. Lü and J. T. Kindt, J. Chem. Phys. **120**, 10328 (2004).
[15] J. T. Kindt, in *Mesoscale Phenomena in Fluid Systems*, edited by F. Case and P. Alexandridis (ACS Symposium Series, 2003), Vol. 861, p. 298.
[16] D. Blankschtein, G. M. Thurston, and G. B. Benedek, Phys. Rev. Lett. **54**, 955 (1985); G. Jackson, W. G. Chapman, and K. E. Gubbins, Mol. Phys. **65**, 1 (1988); J. Dudowicz, K. F. Freed, and J. F. Douglas, J. Chem. Phys. **112**, 1002 (2000); J. T. Kindt and W. M. Gelbart, *ibid.* **114**, 1432 (2001).
[17] A. Ben-Shaul and W. M. Gelbart, in *Micelles, Membranes, Microemulsions, and Monolayers*, edited by W. M. Gelbart, A. Ben-Shaul, and D. Roux (Springer, New York, 1994), p. 1.
[18] P. van der Schoot and M. E. Cates, Europhys. Lett. **25**, 515 (1994).
[19] I. Borukhov, K. C. Lee, R. F. Bruinsma, W. M. Gelbart, A. J. Liu, and M. J. Stevens, J. Chem. Phys. **117**, 462 (2002); A. V. Ermoshkin, A. N. Kudlay, and M. O. de la Cruz, *ibid.* **120**, 11930 (2004).
[20] L. Onsager, Ann. N.Y. Acad. Sci. **51**, 627 (1949).